

Warming-induced vapor pressure deficit suppression of vegetation growth diminished in northern peatlands

Received: 2 February 2023

Accepted: 26 October 2023

Published online: 30 November 2023

 Check for updates

Ning Chen^{1,2}, Yifei Zhang¹, Fenghui Yuan^{1,3}, Changchun Song^{1,4}✉, Mingjie Xu⁵, Qingwei Wang¹✉, Guangyou Hao², Tao Bao⁶, Yunjiang Zuo¹, Jianzhao Liu^{1,7}, Tao Zhang⁵, Yanyu Song¹, Li Sun¹, Yuedong Guo¹, Hao Zhang¹, Guobao Ma¹, Yu Du¹, Xiaofeng Xu¹✉ & Xianwei Wang¹✉

Recent studies have reported worldwide vegetation suppression in response to increasing atmospheric vapor pressure deficit (VPD). Here, we integrate multisource datasets to show that increasing VPD caused by warming alone does not suppress vegetation growth in northern peatlands. A site-level manipulation experiment and a multiple-site synthesis find a neutral impact of rising VPD on vegetation growth; regional analysis manifests a strong declining gradient of VPD suppression impacts from sparsely distributed peatland to densely distributed peatland. The major mechanism adopted by plants in response to rising VPD is the “open” water-use strategy, where stomatal regulation is relaxed to maximize carbon uptake. These unique surface characteristics evolve in the wet soil-air environment in the northern peatlands. The neutral VPD impacts observed in northern peatlands contrast with the vegetation suppression reported in global nonpeatland areas under rising VPD caused by concurrent warming and decreasing relative humidity, suggesting model improvement for representing VPD impacts in northern peatlands remains necessary.

Vegetation dynamics are critical in shaping carbon balances and generating biophysical feedback within the climate system by modifying surface albedo and the energy budget^{1–5}. Vegetation greening was evident before the late 1990s and has now stalled or reversed because of a sharp increase in global vapor pressure deficit (VPD), partially offsetting positive CO₂ fertilization effects⁶. These observations indicate that vegetation greening is usually negatively correlated with increasing VPD^{6–10}. The prolonged period of high VPD has been acknowledged as a major driver of large-scale tree mortality^{11,12}, global

vegetation greening reversal^{7,8,13}, and carbon sink reduction¹³. These negative impacts usually occur with increasing VPD ($VPD = f(Ta, RH)$) caused by warming air temperature (Ta) and declining relative humidity (RH) or are covaried^{6,14}. Although VPD shows a continuously increasing trend after the 1990s^{6,15}, its effects on vegetation and the underlying mechanisms may vary among regions due to different environmental conditions¹⁶.

Although the typically negative VPD effects have been widely discussed recently, the increasing VPD may be driven by different

¹Key Laboratory of Wetland Ecology and Environment, Northeast Institute of Geography and Agroecology, Chinese Academy of Sciences, 130102 Changchun, China. ²CAS Key Laboratory of Forest Ecology and Management, Institute of Applied Ecology, Chinese Academy of Sciences, 110016 Shenyang, China. ³Department of Soil, Water, and Climate, University of Minnesota, Saint Paul, MN 55108, USA. ⁴School of Hydraulic Engineering, Dalian University of Technology, 116024 Dalian, China. ⁵College of Agronomy, Shenyang Agricultural University, 110866 Shenyang, China. ⁶Key Laboratory of Regional Climate-Environment for Temperate East Asia, Institute of Atmospheric Physics, Chinese Academy of Sciences, Beijing, China. ⁷College of Surveying and Exploration Engineering, Jilin Jianzhu University, 130018 Changchun, China. ⁸Biology Department, San Diego State University, San Diego 92182, USA. ✉e-mail: songcc@iga.ac.cn; xxu@sdsu.edu; wangxianwei@iga.ac.cn

mechanisms. A recent global study has detected a subtle increase in RH in northern peatlands over the last four decades¹⁷ (Supplementary Fig. 1), suggesting that the actual water vapor (AVP) increases at approximately the same rate as the saturation water vapor (SVP) ($RH = f(AVP, SVP)$). This may be due to the unique surface characteristics of the water-rich environment and the high moss cover in the northern peatlands, which supplies sufficient atmospheric water to meet the increasing water demand caused by high VPD¹⁸ and to maintain the atmospheric water balance. If RH remains unchanged, warming alone may lead to widespread increases in atmospheric VPD¹⁹. Over the same period of subtle changes in RH and substantial increases in VPD⁶, a neutral response of vegetation growth to VPD has been detected from recent analyses^{6,13,20,21}. Multiple lines of evidence have raised the concern that vegetation growth may respond differently to increasing VPD caused by warming alone, contrasting to that caused by concurrent warming and decreased RH. However, no direct observational evidence has been reported for whether increasing VPD can be driven by warming alone or how vegetation growth responds to warming-induced increases in VPD¹⁶.

The main mechanism behind the VPD effects in the northern peatlands may be different from those in other ecosystems. Increasing atmospheric demand for water induced by rising VPD suppresses photosynthesis and transpiration of plants by controlling stomatal activity and xylem conductance; therefore, increasing VPD plays a critical role in regulating the water and carbon cycles of terrestrial ecosystems^{10,16,22}. VPD can also indicate atmospheric dryness. A typical plant response to increasing VPD is stomatal closure to minimize water loss and avoid excessive water tension within the xylem at the expense of reducing or stopping photosynthesis^{7,10,16,22–24}. It is well known that the vegetation response to increasing VPD is always negative^{6–10,22,25}. In contrast, photosynthesis in the Amazon rainforest increases as the VPD increases²⁶, mainly due to new leaves flushed during the dry season compensating for the stomatal limitations caused by increased atmospheric dryness²⁵. A moist and cold environment combined with high moss cover may produce sufficient atmospheric moisture to meet the increasing water demand caused by increasing VPD in northern peatlands¹⁸, potentially relieving atmospheric dryness^{27,28}. In this wet soil-air environment, plants may adopt an “open” water-use strategy in response to water stress by relaxing stomatal regulation to maximize carbon uptake at the cost of hydraulic risk²⁹.

Here, we compiled multisource datasets of in situ observations, a multisite synthesis (78 sites), eddy covariance flux towers (18 sites from FLUXNET-CH₄ Community Product and 95 sites from FLUXNET2015), and regional-scale remote sensing products to explore the effects of increasing VPD and investigate their underlying mechanisms in northern peatlands. We further compared the northern peatlands with global nonpeatlands to identify the VPD impacts on vegetation in northern peatlands that differ from the prevailing viewpoint of VPD suppression on vegetation. Our data implied that the suppressive effect of rising VPD driven by co-occurring warming and decreasing RH on vegetation growth in the global nonpeatland regions was greater than that caused by warming alone in the northern peatlands. Differences in surface characteristics (e.g., water availability) and plant traits (e.g., plant water-use strategy) were the major factors explaining these contrasting VPD effects.

Results and discussion

Vegetation responses to warming-induced rising VPD in northern peatlands

Synthesized warming experiments showed no suppressive impact of rising VPD on vegetation growth in the northern peatlands. Sixty-seven synthesized warming experiments with observed Ta and vegetation growth and simulated VPD from the CRU 4.04 datasets were extracted from a recent warming meta-analysis across the northern peatlands³⁰. The CRU 4.04 datasets of Ta and VPD matched well with the

observations in 18 eddy covariance towers, with significant correlation coefficients (r) of 0.98 ± 0.03 (mean ± 1 standard error, se) and 0.93 ± 0.02 for Ta and VPD, respectively ($p < 0.05$, Supplementary Fig. 2a, b, Methods). Eddy covariance flux data showed that VPD exponentially increased with Ta ($p < 0.05$, mean ± 1 se, $r = 0.93 \pm 0.01$, Supplementary Fig. 2c, Methods). We then fitted the exponential relationships between Ta and VPD from the CRU 4.04 datasets ($p < 0.05$, mean ± 1 se, $r = 0.91 \pm 0.004$) to simulate VPD differences between the warming and control treatments at 67 sites (Supplementary Table 1, Methods). Regression analyses showed that the warming impacts on net primary productivity (NPP) had no relationship with VPD across sites, suggesting that vegetation in the northern peatlands was not affected by rising VPD (regression coefficients ± 1 se, -0.02 ± 0.08 , $p = 0.769$, Fig. 1a).

Among the observations of VPD and vegetation growth in warming experiments, we found that rising VPD caused by warming alone did not significantly reduce vegetation growth in the northern peatlands. Observational data from a warming experiment in Mohe showed that the warming treatment elevated Ta by 3.8 ± 0.6 °C (mean ± 1 se, $p < 0.001$) and decreased RH by 1.1 ± 0.6 % ($p = 0.096$), leading to a significant increase in VPD of 1.5 ± 0.3 hPa ($p < 0.001$, Fig. 1b–d). However, vegetation growth (measured by canopy conductance, G_c , of *Vaccinium uliginosum*) did not show suppression in response to the increasing VPD caused by warming alone (regression coefficients ± 1 se, 0.23 ± 0.48 , $p = 0.642$, Fig. 1e).

To verify these findings at the Mohe site, we synthesized six other field warming experiments from 273 independent sites in a meta-analysis³⁰. In these warming experiments, Ta, VPD (or RH), and an indicator of vegetation growth, such as biomass, were included in the warming and control treatments (Supplementary Table 2, Methods). Compared with the control treatment, the warming treatments resulted in significant increases in Ta ($p = 0.002$) and insignificant reductions in RH ($p = 0.083$), with values of 2.7 ± 0.6 °C (mean ± 1 se) and 8.0 ± 4.0 %, respectively, leading to a significant increase in VPD of 2.6 ± 1.1 hPa ($p = 0.043$, Fig. 1f–h). The synthesized results confirmed that the growing VPD induced by warming alone did not yield significant suppression impacts on vegetation growth in the northern peatlands (regression coefficients ± 1 se, -0.11 ± 0.27 , $p = 0.701$, Fig. 1i).

We extended the analysis to the northern peatland area to verify the neutral VPD impacts on vegetation activities at a larger scale. Across the entire northern peatlands, Ta (mean ± 1 se, 0.028 ± 0.006 °C yr⁻¹, $p < 0.001$) and VPD (0.004 ± 0.002 hPa yr⁻¹, $p = 0.039$) substantially increased from 1982 to 2018, while RH (0.018 ± 0.010 % yr⁻¹, $p = 0.076$) remained unchanged (Fig. 2a–c). Over the 37 years, more than 60.0% of the regions with significant increases in VPD had significant increases in Ta ($p < 0.05$) but not in RH ($p > 0.05$) over the northern peatlands (Supplementary Fig. 3). Partial correlation (PCOR) analyses showed that the regional mean PCOR coefficients (PCOR_{GPP} vs. VPD) of the three datasets of satellite-derived gross primary productivity (GPP) were 0.06–0.08 (Fig. 2d–f). Three detrended satellite-derived GPP positively correlated with detrended VPD over 58.2 to 66.4% (24.8 to 33.0% with a significant positive correlation at $p = 0.05$) of the northern peatlands when detrended Ta, radiation, wind speed, and precipitation were considered (Fig. 2d–f, Methods). In contrast, a significant negative response of GPP to VPD was found in only 8.1–16.8% of the northern peatlands ($p < 0.05$, Fig. 2d–f). The suppression impact weakened with increasing peatland extent. As the peatland extent increased from 10% to >70%, the regional mean PCOR_{GPP} vs. VPD increased from 0.09 ± 0.01 (mean ± 1 se for three satellite-derived GPP) to 0.17 ± 0.02 , and the percentage of significantly negative PCOR_{GPP} vs. VPD decreased from 8.58 ± 2.35 to 0.81 ± 0.44 (Fig. 2g–l). This further suggested that increasing VPD had a neutral impact on vegetation growth in the northern peatlands, especially for the densely distributed peatlands.

Vegetation responses to rising VPD caused by concurrent warming and decreasing RH in global nonpeatland regions

Increasing VPD caused by concurrent warming and decreasing RH led to a stronger suppression impact on GPP in global nonpeatland regions. Ta (mean \pm 1 se, $0.027 \pm 0.003^\circ\text{C yr}^{-1}$, $p < 0.001$) and VPD ($0.018 \pm 0.001 \text{ hPa yr}^{-1}$, $p < 0.001$) increased significantly during 1982–2018, but RH ($-0.027 \pm 0.005\%$ yr^{-1} , $p < 0.001$) decreased

significantly in global nonpeatland regions (Fig. 3a–c). From 1982 to 2018, ~60% of the global nonpeatland regions showed an increasing VPD trend with significantly increasing Ta and significantly declining RH ($p < 0.05$, Supplementary Fig. 4). When the detrended Ta, radiation, wind speed, and precipitation were considered, PCOR analyses showed that three detrended satellite-derived GPP were negatively correlated with the detrended VPD over 65.7–72.7% of the global

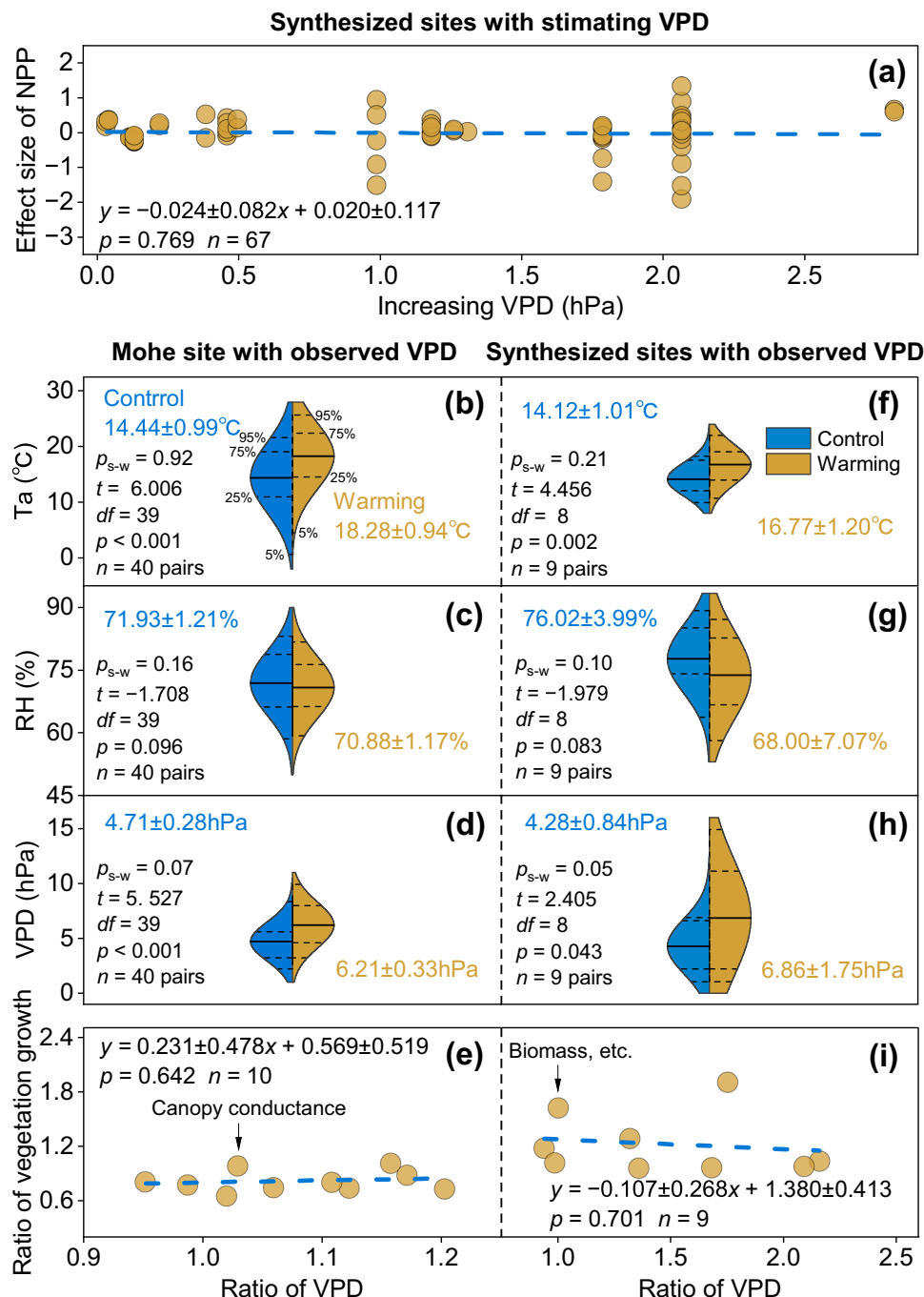


Fig. 1 | Changes in air temperature (Ta), relative humidity (RH), and vapor pressure deficit (VPD) and VPD impacts on vegetation growth. a, e and i VPD impacts on vegetation growth at 67 warming experiment sites stimulating VPD (a), Mohe site (e), and synthesized warming experiment sites (i) with observed VPD under the control and warming treatments. Vegetation growth is quantified as canopy conductance of *Vaccinium uliginosum* at the Mohe site (e) and by biomass (i), etc., at the synthesized sites. Ratio: ratio of vegetation growth and VPD in the warming treatment to the control treatment (e and i). n represents the total

number of observations (a–i). b and f, c and g, d and h Changes in Ta, RH, and VPD under control (blue) and warming (brown) treatments. Black lines indicate the means of Ta, RH, and VPD under warming and control treatments in the violin plots. Dotted lines indicate 5%, 25%, 75%, and 95% percentiles in the violin plots. $p_{s-w} > 0.05$ indicates that differences in Ta, RH, and VPD between warming and control treatments meet the Shapiro–Wilk test for normality. p values, t -statistic (t), and degrees of freedom (df) are the result of t -tests of Ta, RH, and VPD between control and warming treatments.

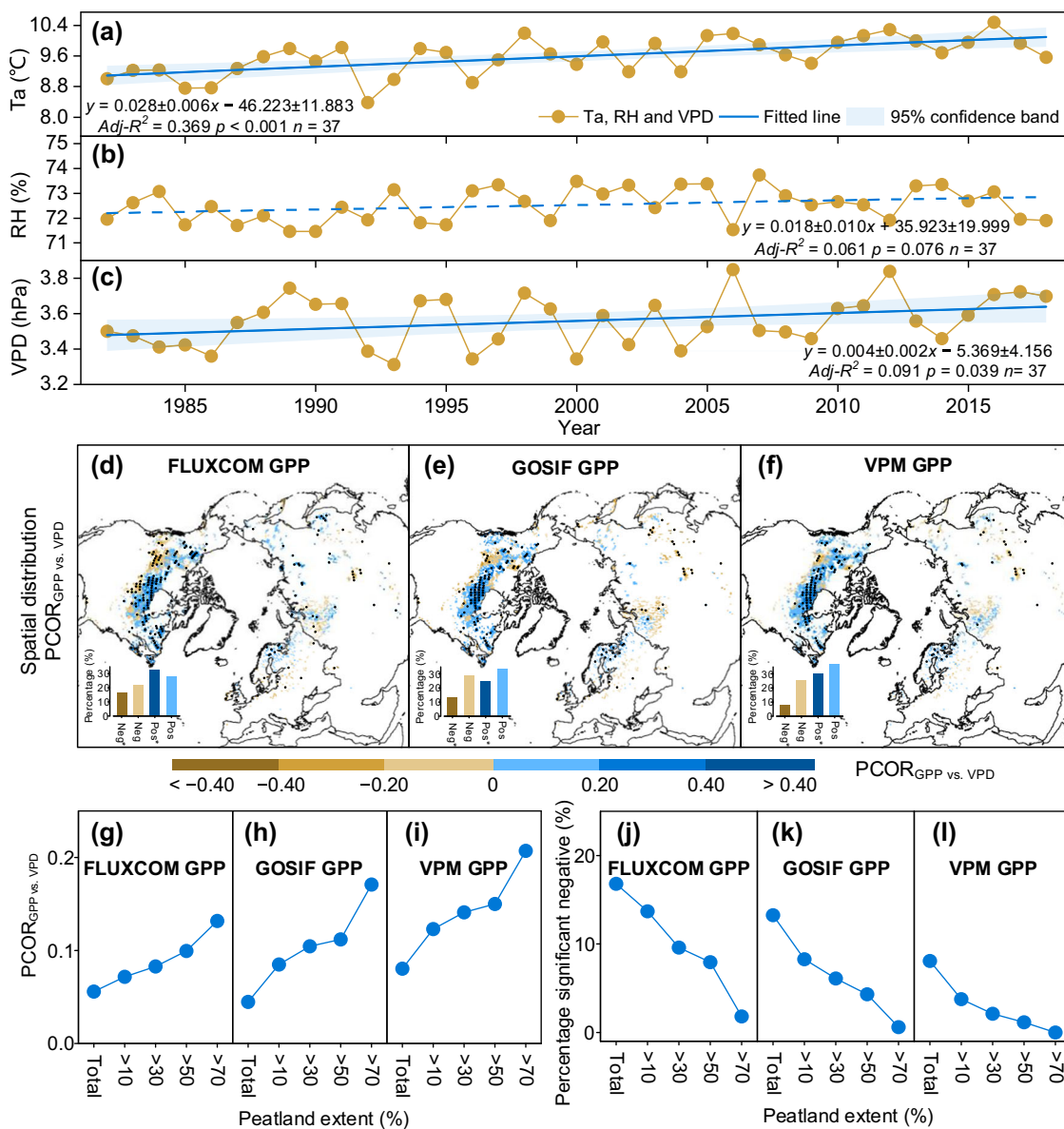


Fig. 2 | Changing rates of air temperature (Ta), relative humidity (RH), vapor pressure deficit (VPD), and spatial distributions of the VPD impacts on vegetation growth across the northern peatlands during 1982–2018. **a–c** Changing rates of Ta, RH, and VPD from 1982 to 2018. Solid and dotted lines indicate the significant and insignificant variability of Ta, RH, and VPD, respectively. Shading areas along the regression lines are the 95% confidence band. $Adj-R^2$: Adjusted R

Square. n represents the total number of observations. **d–f** The spatial distributions of the PCOR_{GPP} vs. VPD derived from FLUXCOM GPP, GOSIF GPP, and VPM GPP. Insets show the percentage (%) of significant (Neg) and insignificant (Pos) negative (brown) PCOR_{GPP} vs. VPD and significant (Pos) and insignificant (Pos) positive (blue) PCOR_{GPP} vs. VPD. **g–l** Changes in regional mean PCOR_{GPP} vs. VPD (**g–i**) and the percentage of significant negative PCOR_{GPP} vs. VPD (**j–l**) across the peatland extent.

nonpeatland regions (44.3–58.2% with a significant negative correlation, $p < 0.05$) (Fig. 3d, Supplementary Fig. 5). The regional mean PCOR_{GPP} vs. VPD ranged from -0.16 to -0.21 for the three satellite-derived GPP (Fig. 3d). The spatial coverage of significantly negative PCOR_{GPP} vs. VPD was 40% higher and the regional mean PCOR_{GPP} vs. VPD was 0.25 lower in the global nonpeatland regions than those in the northern peatlands (Fig. 3d).

To further assess the robustness of the divergent drivers and impacts of increasing VPD, the global nonpeatland regions were divided into nonhumid regions ($AI < 0.65$) and humid regions ($AI \geq 0.65$) based on the aridity index (AI, Methods)³¹. From 1982 to 2018, changes in the temporal trends of Ta, RH, and VPD in the nonhumid regions and the humid regions were consistent with those in the entire nonpeatland region (Supplementary Figs. 4, 6). The PCOR analyses, when the detrended Ta, radiation, wind speed, and precipitation were

considered, showed that the spatial coverage of significantly negative PCOR_{GPP} vs. VPD were 59.5% higher (mean of the three satellite-derived GPP) in the nonhumid regions and 25.4% greater in the humid regions, respectively ($p < 0.05$, Supplementary Figs. 5, 6), than those in the northern peatlands. In addition, a lower regional mean PCOR_{GPP} vs. VPD from three satellite-derived GPP was observed in the nonhumid regions (-0.32) and the humid regions (-0.14) compared to the northern peatlands (0.06) (Supplementary Figs. 5, 6).

The VPD effects based on satellite-derived GPP in the northern peatlands and the global nonpeatland regions were validated by comparison against results with 113 eddy covariance flux towers. Observational data showed that detrended VPD was significantly negatively correlated with detrended GPP at 1 out of 18 (5.6%) eddy covariance flux towers in the northern peatlands and 43 out of 95 (45.3%) towers in global nonpeatland regions, respectively ($p < 0.05$,

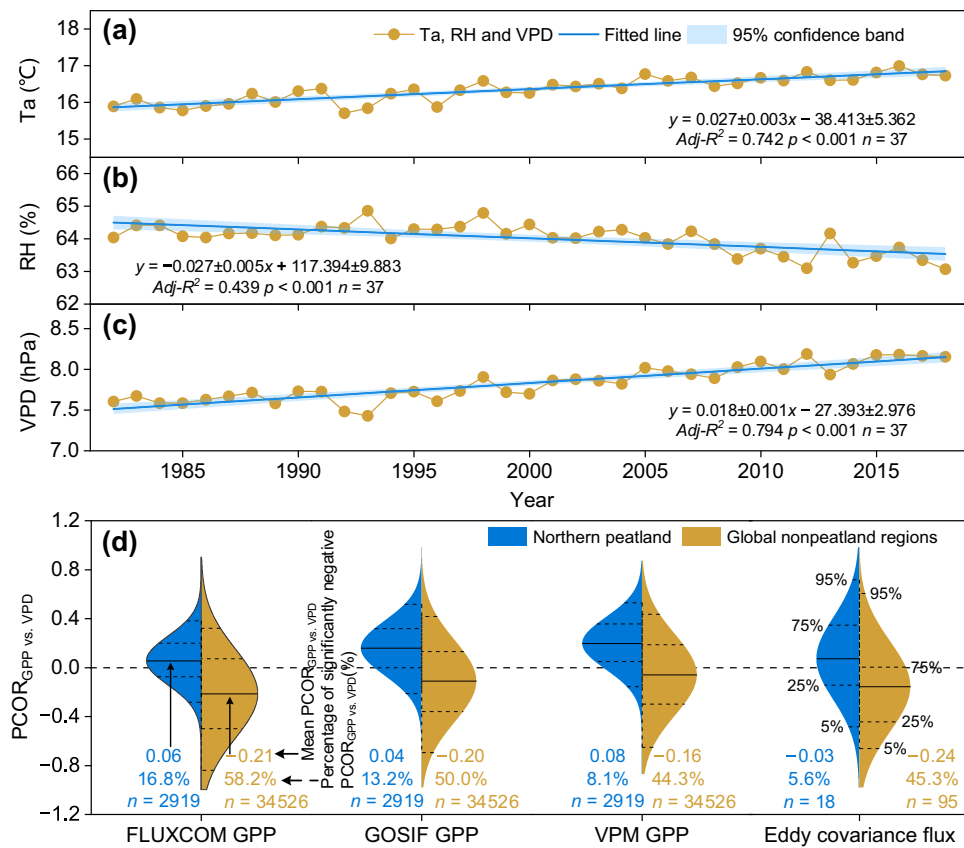


Fig. 3 | Changing rates of air temperature (Ta), relative humidity (RH), and vapor pressure deficit (VPD) and the impact of VPD on vegetation growth in global nonpeatland regions. a–c Changing rates of Ta, RH, and VPD from 1982 to 2018 in global nonpeatland regions. Shading areas along the regression lines are the 95% confidence band. $Adj-R^2$: Adjusted R Square. **d** Differences in VPD effects as estimated by the mean PCOR_{GPP} vs. VPD (horizontal solid arrow direction) and the

percentage (%) of significantly negative PCOR_{GPP} vs. VPD (horizontal dotted arrow direction) between the northern peatlands (blue) and the global nonpeatland regions (brown). Solid lines in the violin plots indicate the mean PCOR_{GPP} vs. VPD. Dotted lines indicate 5%, 25%, 75%, and 95% percentiles in the violin plots. n indicates the total number of observations.

Fig. 3d). Grouping the 95 eddy covariance flux towers into the non-humid regions (33 towers) and the humid regions (62 towers) further confirmed a greater VPD suppression impact in the global nonpeatland regions compared to the northern peatlands, with a significantly negative PCOR_{GPP} vs. VPD of 63.6% and 35.5% in the nonhumid regions and the humid regions, respectively (Supplementary Fig. 6). In addition, according to the latitude, longitude, and time span in 113 eddy covariance flux towers, we found that the symbols (\pm) of the satellite-derived PCOR_{GPP} vs. VPD agreed with 76.4% (mean value from three satellite-derived GPP) of the eddy covariance flux towers (Supplementary Fig. 7, Methods). In addition, the satellite-derived PCOR_{GPP} vs. VPD was positively correlated with eddy covariance PCOR_{GPP} vs. VPD, with r values ranging from 0.51 to 0.58 ($p < 0.05$, Supplementary Fig. 7). In summary, the field-scale and grid-scale observations consistently suggested that the prevailing viewpoint derived from the global nonpeatland regions may overestimate the VPD suppression impact in the northern peatlands.

Mechanisms for the divergent VPD effects

Six plant traits and environmental factors were used to understand the causes of the contrasting VPD effects. Soil hydraulic properties were measured by soil organic carbon (SOC) and bulk density (BD)³². Generally, higher SOC and lower BD indicated good soil hydraulic properties^{32,33}. Climate water deficit (CWD) and available volumetric water content (VWC) were used to evaluate water availability^{34–36}. A low CWD and a high VWC correspond to a wet environment. Plant water-use strategy was quantified by underlying water use efficiency (uWUE)

and transpiration (Et) response to VPD (PCOR_{Et} vs. VPD)³⁷. The uWUE is inversely proportional to the marginal water cost of carbon gain (λ)^{38,39} and is widely used as the proxy for plant water-use strategy^{40–42}. For example, a high uWUE corresponds to a low λ , as a “reduce expenditures” water-use strategy, suggesting that plants tended to close stomata sooner and minimize water loss under drying conditions at the cost of carbon uptake^{37,42}. Overall, in regions where a “reduce expenditure” and an “open” water-use strategy is more prevalent, this is associated with a higher and lower uWUE, respectively^{40,41}. PCOR_{Et} vs. VPD provided a direct proxy for the response of stomatal activity to increasing VPD, with a more positive value indicating weaker stomatal limitation and a more negative value indicating stronger stomatal limitation. In addition, PCOR_{Et} vs. VPD can also be used as a proxy for atmospheric water supply in response to increasing water demand caused by increasing VPD³⁷.

Differing plant water-use strategies were a major reason for the contrasting VPD effects. We used the random forest algorithm - a machine learning approach - to relate the PCOR_{GPP} vs. VPD (a proxy for VPD effects) as a function of six plant traits and environmental factors (Methods). The predicted PCOR_{GPP} vs. VPD from the random forest models agreed well with the observed PCOR_{GPP} vs. VPD ($r = 0.84$ to 0.85 , $p < 0.001$, Fig. 4a). The sensitivity of PCOR_{GPP} vs. VPD to changes in uWUE (mean ± 1 se, -0.80 ± 0.13) and PCOR_{Et} vs. VPD (1.12 ± 0.19) was greater than that of the other variables (-0.71 ± 0.05 to 0.27 ± 0.07) (Fig. 4b, Methods). PCOR_{GPP} vs. VPD decreased with increasing uWUE, but it increased with increasing PCOR_{Et} vs. VPD (Fig. 4b). In the northern peatlands, the uWUE and the PCOR_{Et} vs. VPD were $0.61 \text{ g C kPa}^{0.5} \text{ kg}^{-1}$

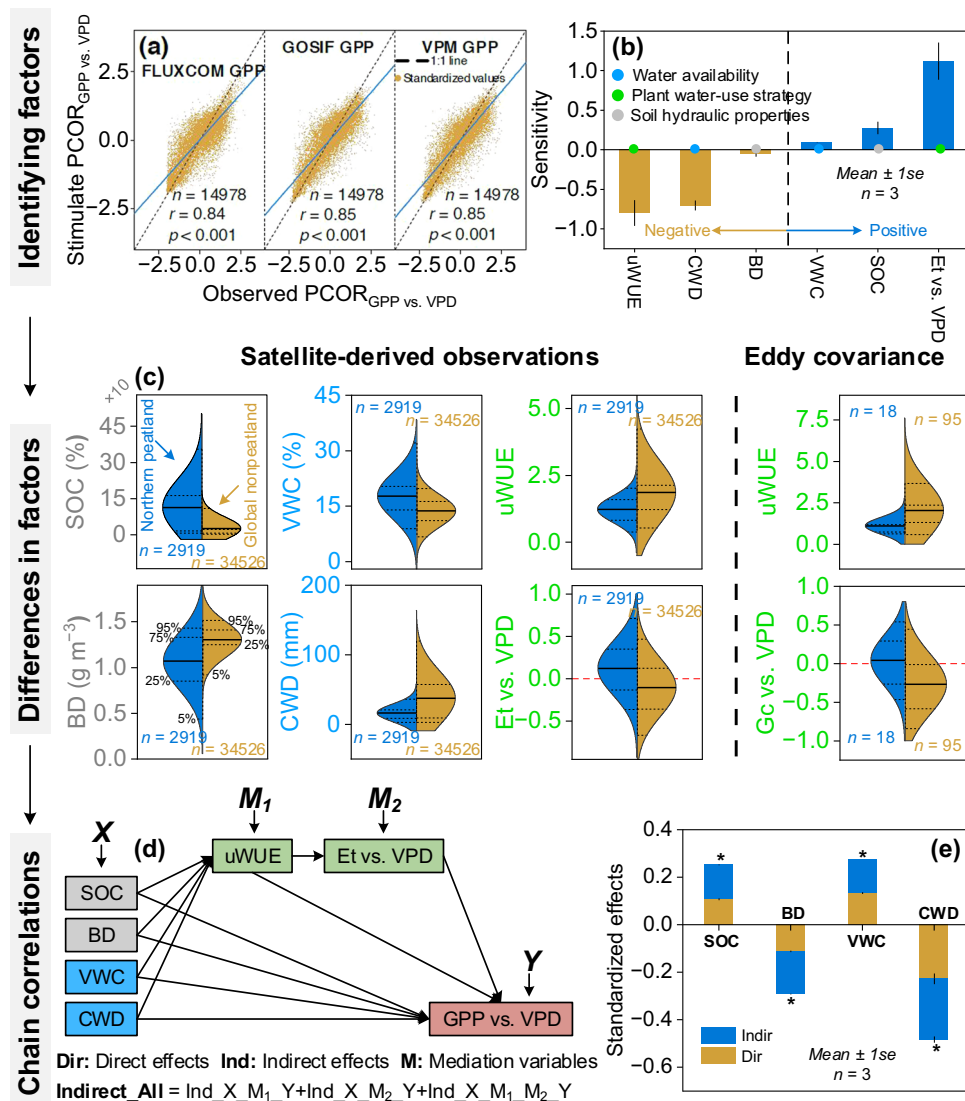


Fig. 4 | Mechanisms for the divergent VPD effects between the northern peatlands and global nonpeatland regions. **a** Correlations of observed PCOR_{GPP} vs. VPD from three satellite-derived GPP datasets with simulated PCOR_{GPP} vs. VPD. **b** Sensitivities (mean \pm 1 standard error; positive: blue histograms; negative: brown histograms) of the PCOR_{GPP} vs. VPD to water availability (VWC and CWD; blue dots), soil hydraulic properties (SOC and BD; gray dots), and plant water-use strategy (PCOR_{ET} vs. VPD and uWUE; green dots). **c** Differences in water availability, soil hydraulic properties, and plant water-use strategy between the northern peatlands and the global nonpeatland regions, including satellite-derived observations (left of dotted line) and eddy covariance flux towers (right of dotted line). Solid lines in the

violin plots indicate the mean of these variables. Dotted lines indicate 5%, 25%, 75%, and 95% percentiles in the violin plots. n indicates the total number of observations. **d** Schematic diagram illustrating the mediation effect models. Ind_{X_M1_Y}, Ind_{X_M2_Y}, and Ind_{X_M1_M2_Y} indicate that water availability (X) and soil hydraulic properties (X) influence the VPD effects (Y , GPP vs. VPD) through uWUE (M_1 , Ind_{X_M1_Y}), PCOR_{ET} vs. VPD (Et vs. VPD; M_2 , Ind_{X_M2_Y}), and both (Ind_{X_M1_M2_Y}). **e** Standardized direct and indirect effects (mean \pm 1 standard error) of water availability and soil hydraulic properties on the VPD effects. “*” denotes that all the standardized effects are significant ($p < 0.05$). Error bars represent one unit of standard error ($n = 3$) (**b** and **e**).

H_2O lower and 0.22 higher than the global nonpeatland regions, respectively (mean \pm 1 se, 1.23 ± 0.01 vs. 1.84 ± 0.01 g C $kPa^{0.5}$ $kg^{-1} H_2O$, 0.13 ± 0.01 vs. -0.09 ± 0.006) (Fig. 4c). Overall, plants in the northern peatlands tended to adopt an “open” water-use strategy with lower uWUE and higher PCOR_{ET} vs. VPD in response to increasing VPD, leading to a weaker suppressive impact on vegetation growth compared to the global nonpeatland regions.

We further assessed the robustness of the satellite-derived differences in the plant traits between the northern peatlands and the global nonpeatland regions using eddy covariance flux towers. As the proxy for the plant water-use strategy, the uWUE in the northern peatlands was 0.78 g C $kPa^{0.5}$ $kg^{-1} H_2O$ lower than that in the global nonpeatland regions (mean \pm 1 se, 1.10 ± 0.12 vs. 1.88 ± 0.10 g C $kPa^{0.5}$ $kg^{-1} H_2O$) (Fig. 4c). Compared to the global nonpeatland regions, weak

stomatal regulation and an abundant atmospheric water supply in response to increasing VPD in the northern peatlands were also confirmed by the eddy covariance flux datasets. For stomatal activity, a significant negative response of G_c to VPD was found in only 5.6% of the eddy covariance flux towers in the northern peatlands (coefficient mean \pm 1 se, 0.04 ± 0.08), whereas this percentage increased to 52.6% in the global nonpeatland regions (-0.27 ± 0.04) ($p < 0.05$, Fig. 4c, Methods). As a proxy for atmospheric water supply with increasing VPD, a significant negative response of evapotranspiration (ET) to VPD was observed in 36.8% of the towers in the global nonpeatland regions (coefficient mean \pm 1 se, -0.16 ± 0.04), but this percentage was 11.1% in the northern peatlands (0.27 ± 0.08) (Supplementary Fig. 8).

In addition to the plant traits, the impact of VPD was also sensitive to the soil hydraulic properties and water availability. PCOR_{GPP} vs. VPD

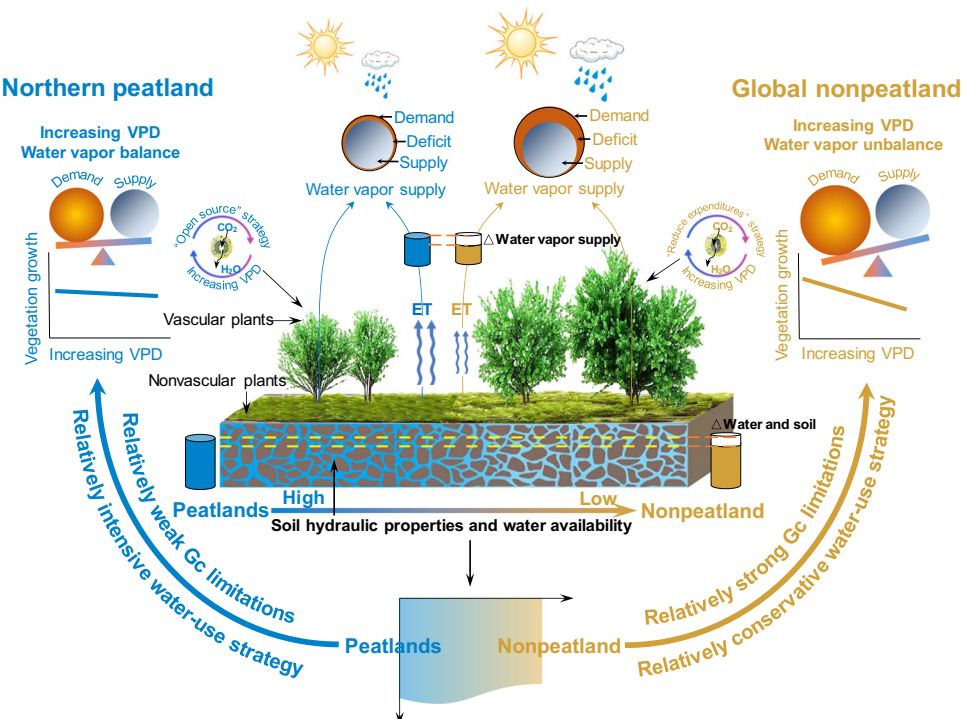


Fig. 5 | Schematic illustrating divergent vegetation responses to rising vapor pressure deficit (VPD) between the northern peatlands and the global non-peatland regions. Compared to the global non-peatland regions, the supply of atmospheric water vapor, deriving from ample soil water availability and high coverage of nonvascular plants (e.g., moss), could meet the water demand of increasing VPD in the northern peatlands, as evidenced by slight changes in relative humidity (RH). In a water-rich environment of the northern peatlands, plants tend to adopt an “open” water-use strategy with increasing VPD, leading to a weak regulation of stomatal activity and, thus, neutral VPD impacts on vegetation growth. Both lines and approximate trapezoids with color gradients from blue to

brown indicate water conditions and soil hydraulic properties from high (or good) to low (or weak). Both pairs of cylinders indicate the differences (white in the cylinders) in water vapor supply (top, Δ water vapor supply) and water conditions and soil hydraulic properties (bottom, Δ water and soil) between northern peatlands and global non-peatland regions. Differences in changes in RH between the northern peatlands and the global non-peatland regions are exhibited by the balance in “supply” (orange circle) and “demand” (blue circle). The left (blue) and right (brown) of the figure indicate the northern peatlands and global non-peatland regions, respectively.

increased with increasing VWC and SOC, but it decreased with increasing BD and CWD (Fig. 4b). Compared to the global non-peatland regions, higher VWC (17.58 ± 0.12 vs. $13.56 \pm 0.02\%$) and SOC (1.11 ± 0.02 vs. $0.26 \pm 0.002\%$) and lower BD (1.06 ± 0.01 vs. $1.30 \pm 0.001 \text{ g m}^{-3}$) and CWD (15.9 ± 0.20 vs. $37.4 \pm 0.20 \text{ mm}$) were observed in the northern peatlands (Fig. 4c). These differences suggested that vegetation in the northern peatlands with good soil hydraulic properties and abundant water availability could resist the atmospheric water stress caused by increasing VPD compared to the global non-peatland regions.

We then assessed the cascading correlations of plant water-use strategy, water availability, and soil hydraulic properties with VPD effects using mediation effect models (Methods). The results showed that the water availability and the soil hydraulic properties significantly influenced the VPD effects by determining the plant water-use strategy ($p < 0.05$, Fig. 4d, e). Specifically, changes in VWC (standardized indirect effect $\pm 1 \text{ se}$ from three datasets of satellite-derived GPP, 0.14 ± 0.001) and SOC (0.15 ± 0.001) had a significant positive indirect effect on PCOR_{GPP} vs. VPD through decreasing uWUE and increasing PCOR_{Et} vs. VPD ($p < 0.05$, Fig. 4d, e). In contrast, a significant negative indirect effect was observed from changes in CWD (-0.26 ± 0.01) and BD (-0.18 ± 0.001) ($p < 0.05$, Fig. 4d, e). Collectively, compared to the global non-peatland regions, plants in the northern peatlands adopted an “open” water-use strategy in response to increasing VPD because of the wet environment, favorable soil hydraulic properties, and adequate atmospheric water supply, resulting in a neutral response of vegetation growth to increasing VPD.

Implications

This study represents one of the first attempts to mechanistically examine the VPD impacts on vegetation growth in northern peatlands. The neutral response of vegetation growth to warming-induced increasing VPD in the northern peatlands (Fig. 5) suggested that the prevailing views of vegetation suppression under increasing VPD are not necessarily the case across the globe. This can be explained by the fact that plants in the wet soil-air environment of the northern peatlands tended to adopt an “open” water-use strategy by relaxing stomatal regulation to maximize carbon uptake even as VPD increases (Fig. 5).

An ample atmospheric water supply, driven by a water-rich environment and high moss cover, was a critical factor in determining whether the increasing VPD was caused by warming alone in the northern peatlands. Factors contributing to the wet environment (e.g., relatively high VWC and low CWD) were the high water table⁴³, snow melt⁴⁴, permafrost thaw⁴⁵, and good soil hydraulic properties (e.g., relatively low BD and high SOC), which could directly accelerate water movement from the underlying surface into the atmosphere to meet the increasing water demand caused by rising VPD²⁸ in the northern peatlands. A high moss cover is another essential contributor to the atmospheric water supply with increasing VPD in the northern peatlands¹⁸. Mosses can store substantial water in their interconnected cavernous structures⁴⁶, yet they fail to minimize water loss under increasing atmospheric water demand due to a lack of stomatal regulatory structures^{47,48}. Combining these characteristics with a large surface area, the water evaporation rate in moss is even higher than in

open water⁴⁷. Under the same environmental conditions, our synthesized observations showed that the ET of moss was significantly greater by $0.43 \pm 0.14 \text{ mm day}^{-1}$ (mean $\pm 1 \text{ se}$) than that of vascular plants ($p=0.009$, Supplementary Fig. 9). The moss-dominated wet system of the northern peatlands allowed ET and Et to increase with increasing VPD¹⁸. Therefore, a sufficient atmospheric water supply allowed increases in AVP in approximately the same proportion as the SVP, leading to increasing VPD induced by warming alone in the northern peatlands.

A neutral response of vegetation growth to warming-induced increased VPD was observed in the northern peatlands. This is contrary to the prevailing views that increasing VPD induced by the coaction of warming and decreased RH markedly depressed vegetation growth in global nonpeatland regions^{6-10,22,49}. A relatively dry environment in the global nonpeatland regions can limit atmospheric water supply under increasing VPD, disrupting the supply-demand balance of atmospheric water conditions and exacerbating atmospheric water stress²⁷. This can increase the hydraulic burden of plants, limiting their stomatal activity to preventing excessive water loss at the expense of photosynthesis^{16,50}. In contrast, the moss-dominated wet system of the northern peatlands can provide adequate atmospheric water to meet the increased water demand caused by increasing VPD. Even if atmospheric water stress occurs as warming-induced VPD increases, the stress may be below the threshold that leads to stomatal closure, as evidenced by the neutral response of Gc, Et, and GPP to increasing VPD. In this wet soil-air environment, plants adopt an “open” water-use strategy in response to water stress, maximizing carbon uptake by relaxing stomatal regulation^{24,29}. Although an “open” water-use strategy may sacrifice hydraulic security, plants in water-rich environments would benefit more from keeping their stomata open to take up carbon than from conserving water^{29,41}. Multisource datasets consistently demonstrated that plants in the northern peatlands were believed to resist increasing VPD driven by warming alone.

Three limitations should be acknowledged when interpreting the VPD effects. First, we used uWUE as a proxy for plant water-use strategy but not a more comprehensive metric to characterize vegetation response to water stress²⁹, such as stomatal safety margin (SSM), because of the data limitations at the grid scale. This alternative was supported by previous studies⁴⁰⁻⁴² and the positive correlation of uWUE with SSM²⁹ ($r=0.61$, $p < 0.001$, Supplementary Fig. 10, Methods). Second, stomatal acclimation allows a high carbon assimilation rate in response to increased VPD, especially in species with an “open” water use strategy¹⁹. Although stomatal acclimation might be a possible mechanism for the neutral VPD effects in the northern peatlands¹⁹, it has not been confirmed by our warming experiment in Mohe. Third, the comparison of the VPD effects was carried out between the northern peatlands and the global nonpeatland regions without a comprehensive analysis of spatial heterogeneity. A preliminary analysis found consistent VPD effects, and their underlying mechanisms (six plant traits and environmental factors, Supplementary Fig. 11) in the entire global nonpeatland regions were consistent with the nonhumid and humid regions. Future studies should be designed to address the spatial heterogeneity in VPD and its contributions to the VPD impacts on vegetation.

In conclusion, our study presented novel empirical evidence that VPD increases driven by warming alone did not necessarily suppress vegetation growth in the northern peatlands. The prevailing views of markedly decreasing vegetation growth with increasing VPD around the world might have overestimated the VPD suppression in the northern peatlands. The divergent VPD effects were caused by differences in water availability and soil hydraulic properties that regulated plant water-use strategy and stomatal activity in response to increasing VPD. Specifically, in global nonpeatland regions with relatively dry soils and air, plants adopted a “reduce expenditure” water-use strategy in response to increasing VPD and subsequently limited vegetation

growth. In the moss-dominated wet system of the northern peatlands, increasing VPD did not usually inhibit vegetation growth because plants evolved an “open” water-use strategy in the wet soil and air environment. Therefore, there is an urgent need to revisit and reframe how we represent vegetation growth under increased VPD in water-rich regions, such as northern peatlands, to accurately quantify and predict the land carbon sink.

Methods

Northern peatland maps

The northern peatlands are mainly distributed in the middle and high latitudes in the Northern Hemisphere ($> 30^\circ\text{N}$), which contain more than 75% of the global peatlands^{51,52}. The spatial distribution of the northern peatlands in this study was derived from PEATMAP⁵¹. The map is the result of a synthesized analysis of geospatial information from various sources at global, regional, and national scales³⁵ and has been used in a recent study⁵³. The peatland extent in PEATMAP is extracted from Peat-ML, a map created using machine learning algorithms⁵².

Field warming experiments

First, we used a synthesized dataset to analyze the response of vegetation growth to increasing VPD from a recent meta-analysis³⁰. Studies in the meta-analysis (1990–2020) were collected by searching Google Scholar and Web of Science. The keywords for the topic search were (a) “plant growth” OR “plant height” OR “plant abundance” OR “plant biomass” OR “belowground biomass” OR “aboveground biomass” OR “biomass” OR “production” OR “net primary productivity” OR “plant response” OR “biogeochemical process” and (b) “warming” OR “experimental warming” OR “elevated temperature” OR “climate change” and (c) “wetland” OR “wet tundra” OR “fen” OR “bog” OR “marsh” OR “swamp” OR “peatland”³⁰. Selected publications followed these criteria: (1) experiments, including warming and control treatments, were conducted over at least one growing season; (2) peatlands could be distinguished as vascular plant-dominated (i.e., graminoids, shrubs) or cryptogam-dominated (i.e., mosses and lichens) based on the original site descriptions or relevant results (i.e., species abundance or biomass); and (3) studies included the variables of means, se, standard deviations and sample sizes in control and warming treatments³⁰. The compiled database contained five response variables: plant abundance, plant height, aboveground net primary productivity, belowground net primary productivity, and NPP. A total of 273 independent sites from 51 studies were collected in the northern peatlands (34.72°N to 78.88°N). In this study, we used the NPP to analyze the vegetation growth response to increasing VPD (67 sites, Supplementary Table 1).

VPD was missing from these 67 synthesized warming experiment sites. We extracted Ta and VPD from the CRU 4.04 datasets at the 67 warming experiment sites (reporting NPP) based on their geographic locations. Similar extractions of environmental variables from the CRU 4.04 datasets have also been reported in recent studies^{6,31}. We found that the Ta and VPD from the CRU 4.04 datasets positively correlated with those from 18 eddy covariance flux towers, with a mean r greater than 0.90. This good performance suggested that the CRU 4.04 datasets can be used to simulate the VPD in the 67 warming experiments. Furthermore, the eddy covariance flux towers and the CRU 4.04 datasets consistently showed that VPD exponentially increased with Ta, with a mean r greater than 0.90 (Supplementary Table 1). Based on the exponential relationships between Ta and VPD as estimated by the CRU 4.04 datasets, we simulated the VPD in the control and warming treatments and then obtained increasing VPD with warming.

We then used the warming experiment sites where the VPD (or RH) had been observed under control and warming treatments to further analyze the response of vegetation growth to increasing VPD.

The warming experiment at the Mohe site was conducted in a peatland in the northern Greater Hinggan Mountains (Tuqiang Forestry Bureau in Mohe city, Heilongjiang Province; 52.93°N, 122.83°E). The peatland is characterized by a humid monsoon climate in a cold temperate zone with a mean annual temperature and precipitation of -3.9°C and 450 mm, respectively. The growing season lasts for *c.* 120 days, from mid-May to mid-September. Four common native plant species in the plant community are *Sphagnum palustre* (SP), *Vaccinium uliginosum* (VU), *Ledum palustre* (LP), and *Carex globularis* (CG)⁵⁴.

Our field experiment in Mohe was set up in July 2020, and the warming treatment was placed in a transparent greenhouse (Supplementary Fig. 12). The control treatment was placed in an ambient environment near the transparent greenhouse. The control and warming treatments included 60 mesocosms (square plastic barrels) ($n=30$ per treatment), and four monocultures (SP, CG, VU, and LP), three mixtures of two species (CG-VU, SP-VU, and SP-LP), two mixtures of three species (SP-VU-LP and CG-VU-LP), and one mixture of four species (SP-CG-VU-LP) were included in the control and warming treatments ($n=3$ per species mixture). To simulate the natural plant community in our experimental site, one mixture of four species (SP-CG-VU-LP) was chosen in our study, and the control and warming treatments included 6 mesocosms (square plastic barrels) ($n=3$ per treatment). The observed species and peat soil columns were transplanted from nearby peatlands into square plastic barrels ($45 \times 45 \times 40$ cm). To guarantee homogeneities in the plants and soils, we implemented the following control measurements⁵⁴. (1) Plants with relatively uniform height and coverage were selected from nearby natural peatlands. On the same day, we cleaned the selected plants by removing soil particles under running water and then weighed these plants. We found that the wet weight of the selected plants showed no significant differences between the warming (mean ± 1 se, $476.2 \pm 21.2 \text{ g m}^{-2}$) and control ($451.6 \pm 23.1 \text{ g m}^{-2}$) treatments ($p=0.477$, Supplementary Fig. 13). (2) The square plastic barrels were filled with peat soils (thickness of 30–35 cm) and manually collected in the peatlands from which the plants were sourced. Soil total carbon (TC, 346.0 ± 9.1 vs. $336.5 \pm 4.0 \text{ mg g}^{-1}$, $p=0.393$) and total nitrogen (TN, 27.8 ± 0.5 vs. $28.9 \pm 1.7 \text{ mg g}^{-1}$, $p=0.578$) showed insignificant differences between the warming and control treatments (Supplementary Fig. 13). Additionally, the water in the control treatment was entirely supplied by precipitation. For the warming treatment, precipitation was collected in a container and then evenly sprinkled on each square plastic barrel in the transparent greenhouse after precipitation events⁵⁴. The mean soil moisture content (SMC, %) in the warming treatment decreased insignificantly by 2.0% (33.3 ± 0.5 vs. $31.3 \pm 0.7\%$, $p=0.073$) compared to the control treatment in the growing season of 2021 (Supplementary Fig. 13).

At the Mohe site, TC and TN were detected using a TC-TN analyzer (Shimadzu, Tokyo, Japan). Ta, RH, VPD, and G_c in the 2021 growing season were used to investigate the variability of the environmental variables and the response of vegetation growth (e.g., G_c) to increasing VPD. Ta and RH were measured by a portable temperature and humidity sensor (STM, METER Group Inc.) attached to a data logger (EMSO/G, METER Group Inc.). These indicators were recorded at 30 min intervals. We installed the two sensors in each treatment ($n=2$ per treatment) and took their average. VPD was calculated from Ta and RH using Eq. (1).

$$\text{VPD}(\text{hPa}) = 6.11 \times \exp\left(\frac{17.27 \times \text{Ta}(\text{°C})}{\text{Ta}(\text{°C}) + 273.3}\right) \times \left(1 - \frac{\text{RH}(\%)}{100}\right) \quad (1)$$

G_c , as a proxy for the vegetation growth of *Vaccinium uliginosum*, was measured by an AP4 Porometer (AP4, Delta-t, UK). We measured five leaves of *Vaccinium uliginosum* in each mesocosm (square plastic barrel) under the control and warming treatments. In the peak growing season, diurnal dynamic measurements (9 AM, 14 PM, 17 PM; China

Standard Time) were conducted on August 9 and 18, 2021. Ta and RH were simultaneously measured by an AP4 Porometer.

We further collected another 6 field warming experiments from the northern peatlands to test the robustness of the findings at the Mohe site (Supplementary Table 2). Studies for these field warming experiments were selected from a recent meta-analysis in the northern peatlands, as previously mentioned³⁰. Studies in this analysis were only selected if Ta and RH (or VPD) and vegetation growth (i.e., biomass), in control and warming treatments, were provided. Following these criteria, 6 studies were included in our synthesized analyses.

Satellite and eddy covariance flux datasets

To further investigate whether observations from the field experiments were appropriate for a regional scale, satellite data was used in this study. Monthly solar radiation was derived from the reanalysis products of ERA5-Land ($0.1^{\circ} \times 0.1^{\circ}$)⁵⁵. The monthly wind speed was obtained from TerraClimate (1/24th degree)³⁶. Monthly Ta, precipitation, and AVP were obtained from CRU 4.04 datasets (land; $0.5^{\circ} \times 0.5^{\circ}$)⁵⁶. Monthly SVP and VPD ($0.5^{\circ} \times 0.5^{\circ}$) were calculated by Eqs. (2) and (3), respectively⁶. Recently, the CRU 4.04 datasets have been widely applied to analyze the temporal changes in the trends of VPD and its impact on vegetation growth^{6,13,15,16,20}. Monthly RH was the ratio between AVP and SVP. The ratio of precipitation to potential evapotranspiration was defined as AI (arid and semiarid and dry subhumid regions, $\text{AI} < 0.65$; humid, $\text{AI} \geq 0.65$) (Global-AL_PET_v3)⁵⁷.

$$\text{SVP}(\text{hPa}) = 6.11 \times \exp\left(\frac{17.27 \times \text{Ta}(\text{°C})}{273.3 + \text{Ta}(\text{°C})}\right) \quad (2)$$

$$\text{VPD}(\text{hPa}) = \text{SVP}(\text{hPa}) - \text{AVP}(\text{hPa}) \quad (3)$$

Three satellite-derived GPP products were used to detect vegetation responses to VPD. The monthly Vegetation Photosynthesis Model (VPM) GPP dataset from 2001 to 2018 is based on an improved theory of light use efficiency and applies a state-of-the-art vegetation index gap-filling and smoothing algorithm and a separate treatment of C3/C4 photosynthetic pathways ($0.05^{\circ} \times 0.05^{\circ}$)⁵⁸. It is driven by satellite data from the Moderate-resolution Imaging Spectroradiometer (MODIS) and climate data from the National Centers for Environmental Prediction (Reanalysis II). Solar-induced chlorophyll fluorescence observed by the Orbiting Carbon Observatory-2 (OCO-2) has offered unprecedented opportunities for monitoring land photosynthesis. GOSIF GPP from 2001 to 2018 is produced by GOSIF and linear relationships between solar-induced chlorophyll fluorescence and GPP to map GPP globally at a 0.05° spatial resolution and an 8-day time step⁵⁹. The monthly FLUXCOM GPP product from 1982 to 2015 is produced by using machine learning algorithms to merge carbon flux measurements from FLUXNET eddy covariance flux towers with remote sensing and meteorological data ($0.5^{\circ} \times 0.5^{\circ}$)⁶⁰. Three satellite-derived GPP products have been widely used to analyze VPD effects globally^{13,20,21}.

ET and Et were used to estimate the variables in the random forest models. The MOD16A2 Version 6 ET product is an 8-day composite dataset produced at 500 m pixel resolution. The algorithm of the MOD16 data product collection is based on the Penman–Monteith equation. Inputs included daily meteorological reanalysis data along with MODIS remotely sensed data products such as vegetation property dynamics, albedo, and land cover⁶¹. The dataset of Et was estimated by a coupled diagnostic biophysical model (Penman–Monteith–Leuning model, PML-v2, 500 m, 8 days)⁶². PML-v2 is developed by coupling the widely used photosynthesis model and a canopy stomatal conductance model with the Penman–Monteith energy balance equation⁶². The datasets mentioned above were aggregated to a spatial resolution of 0.5° and temporal resolution of 1 month from 1982 to 2018.

The flux tower-based GPP, latent heat flux (LE, W m^{-2}), sensible heat flux (H, W m^{-2}), and environmental variables of Ta, VPD, precipitation, shortwave radiation, wind speed (m s^{-1}), friction velocity (u_g , unitless), and atmospheric pressure were obtained from the global eddy-covariance flux dataset, FLUXNET2015 (global nonpeatland regions) and FLUXNET-CH₄ Community Product (northern peatlands). Following recent studies on VPD effects, we used GPP estimates based on the nighttime partitioning method (i.e., "GPP_NT_VUT_REF")^{7,20}. We identified and used sites with at least 3 years (more than 15 months) of high-quality data ($\geq 75\%$ of good quality data in a month)⁶³. In addition, we removed all cropland towers in the study area to exclude the effects of human activity⁷. Collectively, we compiled a database consisting of 113 flux tower sites (FLUXNET2015, 95 sites; FLUXNET-CH₄ Community Product, 18 sites). More detailed information on these sites is given in Supplementary Tables 3 and 4, including site name, site coordinates (latitude/longitude), start year of measurements and end year of measurements. The aforementioned variables from satellite and eddy-covariance flux datasets were chosen in the growing seasons from 1982 to 2018. Following a recent study⁶, the growing season was defined as the month in which the mean Ta was greater than zero.

Flux tower-based G_c (mm s^{-1}) was calculated by rearranging the Penman-Monteith equation using the following formula (Eqs. 4 and 5)^{64,65}.

$$G_c = \left[\left(\frac{\Delta}{\gamma} \times \frac{H}{LE} - 1 \right) \times \gamma_a + \frac{\rho C_p}{\gamma} \times \frac{VPD}{LE} \right]^{-1} \quad (4)$$

where Δ is the ratio of the change in SVP to Ta (Pa K^{-1}); γ is the psychometric constant (Pa K^{-1}); ρ is the air density (kg m^{-3}); C_p is the specific heat of air at constant pressure ($\text{J kg}^{-1} \text{K}^{-1}$). Following a previous study⁷ in Eq. 5, γ_a is the aerodynamic resistance (s m^{-1}); k is the von Kármán constant ($k = 0.4$); and ws is the wind speed.

$$\gamma_a = (ws \times k^2) / \log \left(\exp \left(\frac{k \times ws}{u_s} \right) - 0.7 \right)^2 \quad (5)$$

uWUE was estimated by Eq. (6)⁴¹. ET ($\text{kg H}_2\text{O m}^{-2} \text{s}^{-1}$) was converted from LE (W m^{-2}) with a coefficient of $2.44 \text{ J kg}^{-1} \text{ H}_2\text{O}$. To further demonstrate the uWUE as a proxy for plant water-use strategy, we collected the SSM (the difference between water potential at 88% loss of stomatal conductance and the water potential causing 50% loss of hydraulic conductivity) in 133 species in 44 sites from a recent meta-analysis²⁹ and found that uWUE significantly increased with increasing SSM ($r = 0.61$, $p < 0.001$, Supplementary Fig. 10). More detailed information on these SSM sites can be found in a recent study²⁹.

$$uWUE(\text{g C kPa}^{0.5} \text{ kg}^{-1} \text{ H}_2\text{O}) = \frac{GPP(\text{g C m}^{-2}) \times \sqrt{VPD(\text{kPa})}}{ET(\text{kg H}_2\text{O m}^{-2})} \quad (6)$$

The flux tower-based data were used to evaluate the robustness of the VPD effects from the satellite-based datasets based on the PCOR analysis. According to the latitude, longitude, and time span from eddy covariance flux towers, we extracted grid environment variables, FLUXCOM GPP, VPM GPP, and GOSIF GPP. We then compared the VPD effects estimated from eddy covariance flux towers and satellite-based datasets. It should be noted that GOSIF GPP is completely independent of climate data; therefore, it might be more reliable than the other two products in assessing VPD impacts on vegetation growth.

Variables in the random forest models

Six variables were used as predication factors in the random forest models, including BD, SOC, CWD, VWC, uWUE, and PCOR_{Et vs. VPD}. The BD, SOC, and VWC are derived from the gridded Global Soil Dataset (GSD) based on the Soil Map of the World and various regional and national soil databases, including soil attribute data and soil maps³².

The dataset is 30 arc seconds (-1 km at the equator). The vertical distributions of these soil properties ranged from 0 to 2.296 m (8 layers). We selected the soil properties in the 0-0.289 m (1–4 layers) and 0–1.383 m (1–7 layers) soil profiles for the grassland and forest (or shrubland), respectively. The land classifications were obtained from GLASS-GLC at 5 km resolution⁶⁶. The available VWC differed between the VWC at -10 kPa (field capacity) and -1500 kPa (permanent wilting point) soil matric potential³³. uWUE was estimated by CRU VPD and MODIS ET, GPP (Eq. 6). PCOR_{Et vs. VPD} was assessed by PML Et and CRU VPD based on the PCOR analyses. CWD was derived from TerraClimate datasets and is calculated using a water balance model incorporating reference evapotranspiration, precipitation, temperature, and interpolated plant extractable soil water capacity³⁶.

Synthesized comparative observations of ET between vascular plants and mosses

We compared ET between vascular plants and mosses and further investigated the mechanisms of the divergent drivers and impacts of increasing VPD. Studies included in this meta-analysis (1990–2022) were collected by searching Web of Science and Google Scholar for the following keywords: (a) "moss" OR "sphagnum" AND (b) "shrub" OR "graminoid" OR "vascular plant" AND (c) "evapotranspiration" OR "evaporation" OR "water loss". Selected publications had the following criteria: (1) ET was observed in the northern peatlands; (2) ET (mm day^{-1}) of vascular plants and mosses was simultaneously observed in the same environmental conditions; and (3) these observations were conducted for at least one growing season. Following these criteria, 16 comparative data pairs from 5 studies were included in this synthesized analysis (Supplementary Table 5).

Statistical analyses

A paired *t*-test was applied to estimate the effects of warming on RH, Ta, and VPD at the Mohe site and the other 6 synthesized sites by the *t.test* function and to assess the differences in ET between vascular plants and mosses. Shapiro-Wilk was calculated by the *shapiro.test* function and was used to test the normal distributions of differences in these variables between the control and warming treatments. If study variables did not fit the normal distributions, we used a nonparametric test. Due to RH, Ta, and VPD being measured by two repetitions in each treatment at the Mohe site, we could not use the commonly accepted one-way analysis of variance to examine statistical differences in these variables between the control and warming treatments. Differences in biomass, TN, TC, and SMC between the control and warming treatments at the Mohe site were tested by one-way analysis of variance.

A least squares linear regression approach was used to detect temporal changes in the trends of Ta, RH, and VPD from 1982 to 2018 using the *lm* function (Eq. 7).

$$y = \beta_0 + \beta_1 \times t + \varepsilon \quad (7)$$

where y is Ta, RH, and VPD; t is the year; β_0 and β_1 are the regression coefficients, and the investigated variable linear trend is β_1 ; and ε is the residual of the fit. These coefficients were estimated by least squares linear regression.

We used PCOR analyses to assess the impacts of VPD on GPP, ET, and Et using satellite data and eddy-covariance flux data when Ta, precipitation, wind speed, and radiation were considered. In the PCOR analyses, all the variables were detrended by the *detrend* function (trend type = "linear") in the *pracma* package. We implemented the PCOR analyses using the *pcor.test* function in the *ppcor* package.

Random forest models were applied to parse the sensitivity of the VPD effects to plant traits and environmental factors using the *randomForest* function in the *randomForest* package. Sixty percent of the data were used to train the models, and the remaining 40% were used for validation. *r* was used to assess the performance of the simulations,

and the mean r was >0.8 in this study. In the analyses, one of the predictor variables was perturbed by one standard deviation (a value of 1 due to the initial input data normalization), and PCOR_{GPP} vs. VPD was predicted again using the existing random forest model with the predictors including the perturbed ones; this process was repeated for each predictor variable. The predicted PCOR_{GPP} vs. VPD was obtained with and without perturbation, and then we compared it to determine the differences in the sensitivity of the VPD effects to changes in the predictor variables. The calculation of VPD effect sensitivity to plant traits and environmental factors is shown in Eq. (8)^{7,26}. Sensitivity analyses were repeated 15 times, and the median was used in our study.

$$Sensitivity_{VPD\ effects} = \text{median} \left[\frac{\text{Perturbed PCOR}_{GPP\ vs.\ VPD} - \text{No Perturbed PCOR}_{GPP\ vs.\ VPD}}{\text{stdev}(\text{No normalization PCOR}_{GPP\ vs.\ VPD})} \right] \quad (8)$$

Mediation effect models based on the function *PROCESS* (*bruceR* package) were used to investigate the cascading correlations in which the water variability and soil hydraulic properties influenced the VPD effects by affecting the plant water-use strategy. The mediation effect model can test a hypothetical causal chain where one variable X (independent variable) affects a second variable M (mediator) and, in turn, that variable affects a third variable Y (dependent variable). In this model, the independent variables were grid VWC and CWD (water availability), BD and SOC (soil hydraulic properties), the mediators were grid PCOR_{Et} vs. VPD, and uWUE (plant water-use strategy), and the dependent variable was grid PCOR_{GPP} vs. VPD (VPD effects).

Reporting summary

Further information on research design is available in the Nature Portfolio Reporting Summary linked to this article.

Data availability

The datasets used in this study have been deposited in the public data repository (<https://figshare.com/s/a1b39bfc3a2077cc0515>) (Supplementary Table 6).

Code availability

The data in this study were analyzed with publicly available tool packages in R 4.3.0. All the scripts for data analyses are available at <https://figshare.com/s/a1b39bfc3a2077cc0515>.

References

1. Bonan, G. B., Pollard, D. & Thompson, S. L. J. N. Effects of boreal forest vegetation on global climate. *Nature* **359**, 716–718 (1992).
2. Haberl, H. et al. Quantifying and mapping the human appropriation of net primary production in earth's terrestrial ecosystems. *Proc. Natl Acad. Sci.* **104**, 12942–12947 (2007).
3. Shen, M. et al. Evaporative cooling over the Tibetan Plateau induced by vegetation growth. *Proc. Natl Acad. Sci.* **112**, 9299–9304 (2015).
4. Lawrence, M. G. The Relationship between Relative Humidity and the Dewpoint Temperature in Moist Air: A Simple Conversion and Applications. *Bull. Am. Meteorol. Soc.* **86**, 225–234 (2005).
5. Rawson, H. M. & Woodward, J. E. B. G. The effect of atmospheric humidity on photosynthesis, transpiration and water use efficiency of leaves of several plant species. *Planta* **134**, 5–10 (1977).
6. Yuan, W. et al. Increased atmospheric vapor pressure deficit reduces global vegetation growth. *Sci. Adv.* **5**, eaax1396 (2019).
7. Fu, Z. et al. Atmospheric dryness reduces photosynthesis along a large range of soil water deficits. *Nat. Commun.* **13**, 989 (2022).
8. Liu, L. et al. Soil moisture dominates dryness stress on ecosystem production globally. *Nat. Commun.* **11**, 4892 (2020).
9. Sulman, B. N. et al. High atmospheric demand for water can limit forest carbon uptake and transpiration as severely as dry soil. *Geophys. Res. Lett.* **43**, 9686–9695 (2016).
10. Novick, K. A. et al. The increasing importance of atmospheric demand for ecosystem water and carbon fluxes. *Nat. Clim. Change* **6**, 1023–1027 (2016).
11. Williams, A. P. et al. Temperature as a potent driver of regional forest drought stress and tree mortality. *Nat. Clim. Change* **3**, 292–297 (2013).
12. Bauman, D. et al. Tropical tree mortality has increased with rising atmospheric water stress. *Nature* **608**, 528–533 (2022).
13. He, B. et al. Worldwide impacts of atmospheric vapor pressure deficit on the interannual variability of terrestrial carbon sinks. *Natl. Sci. Rev.* **9**, nwab150 (2022).
14. Cheng, Y. et al. A shift in the dominant role of atmospheric vapor pressure deficit and soil moisture on vegetation greening in China. *J. Hydrol.* **615**, 128680 (2022).
15. Fang, Z., Zhang, W., Brandt, M., Abdi, A. M. & Fensholt, R. Globally Increasing Atmospheric Aridity Over the 21st Century. *Earth's Future* **10**, e2022EF003019 (2022).
16. Grossiord, C. et al. Plant responses to rising vapor pressure deficit. *N. Phytol.* **226**, 1550–1566 (2020).
17. Vicente-Serrano, S. M. et al. Recent changes of relative humidity: regional connections with land and ocean processes. *Earth Syst. Dyn.* **9**, 915–937 (2018).
18. Helbig, M. et al. Increasing contribution of peatlands to boreal evapotranspiration in a warming climate. *Nat. Clim. Change* **10**, 555–560 (2020).
19. Marchin, R. M., Broadhead, A. A., Bostic, L. E., Dunn, R. R. & Hoffmann, W. A. Stomatal acclimation to vapour pressure deficit doubles transpiration of small tree seedlings with warming. *Plant Cell Environ.* **39**, 2221–2234 (2016).
20. Song, Y., Jiao, W., Wang, J. & Wang, L. Increased Global Vegetation Productivity Despite Rising Atmospheric Dryness Over the Last Two Decades. *Earth's Future* **10**, e2021EF002634 (2022).
21. Zhong, Z. et al. Disentangling the effects of vapor pressure deficit on northern terrestrial vegetation productivity. *Sci. Adv.* **9**, eadf3166 (2023).
22. Konings, A. G., Williams, A. P. & Gentine, P. Sensitivity of grassland productivity to aridity controlled by stomatal and xylem regulation. *Nat. Geosci.* **10**, 284–288 (2017).
23. Running, S. W. Environmental control of leaf water conductance in conifers. *Can. J. For. Res.* **6**, 104–112 (1976).
24. Rogiers, S. Y. et al. Stomatal response of an anisohydric grapevine cultivar to evaporative demand, available soil moisture and abscisic acid. *Tree Physiol.* **32**, 249–261 (2012).
25. Ding, J. et al. Increasingly important role of atmospheric aridity on Tibetan alpine grasslands. *Geophys. Res. Lett.* **45**, 2852–2859 (2018).
26. Green, J., Berry, J., Ciais, P., Zhang, Y. & Gentine, P. J. S. A. Amazon rainforest photosynthesis increases in response to atmospheric dryness. *Sci. Adv.* **6**, eabb7232 (2020).
27. Martin, J. et al. Recent decline in the global land evapotranspiration trend due to limited moisture supply. *Nature* **467**, 951–954 (2010).
28. Seneviratne, S. I. et al. Investigating soil moisture–climate interactions in a changing climate: A review. *Earth-Sci. Rev.* **99**, 125–161 (2010).
29. Jin, Y. et al. Aridity-dependent sequence of water potentials for stomatal closure and hydraulic dysfunctions in woody plants. *Glob. Change Biol.* **29**, 2030–2040 (2023).
30. Bao, T., Jia, G. & Xu, X. Warming enhances dominance of vascular plants over cryptogams across northern wetlands. *Glob. Change Biol.* **28**, 4097–4109 (2022).

31. Li, X. et al. Temporal trade-off between gymnosperm resistance and resilience increases forest sensitivity to extreme drought. *Nat. Ecol. Evol.* **4**, 1075–1083 (2020).

32. Shangguan, W., Dai, Y., Duan, Q., Liu, B. & Yuan, H. A global soil data set for earth system modeling. *J. Adv. Modeling Earth Syst.* **6**, 249–263 (2014).

33. Huang, L. & Shao, M. A. Advances and perspectives on soil water research in China's Loess Plateau. *Earth-Sci. Rev.* **199**, 102962 (2019).

34. Kustas, W. P. et al. Evaluation of Drought Indices Based on Thermal Remote Sensing of Evapotranspiration over the Continental United States. *J. Clim.* **24**, 2025–2044 (2011).

35. Liu, Y. et al. Identifying a transition climate zone in an arid river basin using the evaporative stress index. *Nat. Hazards Earth Syst. Sci.* **19**, 2281–2294 (2019).

36. Abatzoglou, J. T., Dobrowski, S. Z., Parks, S. A. & Hegewisch, K. C. TerraClimate, a high-resolution global dataset of monthly climate and climatic water balance from 1958–2015. *Sci. Data* **5**, 170191 (2018).

37. Cowan I. R. Regulation of Water Use in Relation to Carbon Gain in Higher Plants. In: *Physiological Plant Ecology II: Water Relations and Carbon Assimilation* (eds Lange O. L., Nobel P. S., Osmond C. B., Ziegler H.). (Springer Berlin Heidelberg, 1982).

38. Zhou, S., Yu, B., Huang, Y. & Wang, G. The effect of vapor pressure deficit on water use efficiency at the subdaily time scale. *Geophys. Res. Lett.* **41**, 5005–5013 (2014).

39. Farquhar, G. D., von Caemmerer, S. V. & Berry, J. A. A biochemical model of photosynthetic CO₂ assimilation in leaves of C 3 species. *Planta* **149**, 78–90 (1980).

40. Beer, C. et al. Temporal and among-site variability of inherent water use efficiency at the ecosystem level. *Glob. Biogeochem. Cycles* **23**, GB2018 (2009).

41. Konings, A. G. & Gentine, P. Global variations in ecosystem-scale isohydricity. *Glob. Change Biol.* **23**, 891–905 (2017).

42. Attia, Z., Domec, J. C., Oren, R., Way, D. A. & Moshelion, M. Growth and physiological responses of isohydric and anisohydric poplars to drought. *J. Exp. Bot.* **66**, 4373–4381 (2015).

43. Carpino, O. A., Berg, A. A., Quinton, W. L. & Adams, J. R. Climate change and permafrost thaw-induced boreal forest loss in north-western Canada. *Environ. Res. Lett.* **13**, 084018 (2018).

44. Qi, W., Feng, L., Liu, J. & Yang, H. Snow as an important natural reservoir for runoff and soil moisture in Northeast China. *J. Geophys. Res.: Atmos.* **125**, e2020JD033086 (2020).

45. Helbig, M. et al. Regional atmospheric cooling and wetting effect of permafrost thaw-induced boreal forest loss. *Glob. Change Biol.* **22**, 4048–4066 (2016).

46. Admiral, S. W. & Lafleur, P. M. Partitioning of latent heat flux at a northern peatland. *Aquat. Bot.* **86**, 107–116 (2007).

47. Heijmans, M. M. P. D., Arp, W. J. & Chapin, F. S. Controls on moss evaporation in a boreal black spruce forest. *Glob. Biogeochem. Cycles* **18**, GB2004 (2004).

48. Williams, T. G. & Flanagan, L. B. Effect of changes in water content on photosynthesis, transpiration and discrimination against ¹³CO₂ and ¹³CO₂ in *Pleurozium* and *Sphagnum*. *Oecologia* **108**, 38–46 (1996).

49. Chen, N. et al. Multiple-scale negative impacts of warming on ecosystem carbon use efficiency across the Tibetan Plateau grasslands. *Glob. Ecol. Biogeogr.* **30**, 398–413 (2020).

50. Oren, R. et al. Survey and synthesis of intra- and interspecific variation in stomatal sensitivity to vapour pressure deficit. *Plant, Cell Environ.* **22**, 1515–1526 (1999).

51. Xu, J., Morris, P. J., Liu, J. & Holden, J. PEATMAP: Refining estimates of global peatland distribution based on a meta-analysis. *Catena* **160**, 134–140 (2018).

52. Melton, J. R. et al. A map of global peatland extent created using machine learning (Peat-ML). *Geosci. Model Dev.* **15**, 4709–4738 (2022).

53. Chaudhary, N. et al. Modelling past and future peatland carbon dynamics across the pan-Arctic. *Glob. Change Biol.* **26**, 4119–4133 (2020).

54. Zhang, Y. et al. Warming effects on the flux of CH₄ from peatland mesocosms are regulated by plant species composition: Richness and functional types. *Sci. Total Environ.* **806**, 150831 (2022).

55. Dee, D. P. et al. The ERA-Interim reanalysis: Configuration and performance of the data assimilation system. *Q. J. R. Meteorol. Soc.* **137**, 553–597 (2011).

56. Viovy N. CRUNCEP Version 7 - Atmospheric Forcing Data for the Community Land Model. Research Data Archive at the National Center for Atmospheric Research, Computational and Information Systems Laboratory. <https://doi.org/10.5065/PZ8F-F017>. Accessed 15 November 2021. (2018).

57. Zomer, R. J., Xu, J. & Trabucco, A. Version 3 of the Global Aridity Index and Potential Evapotranspiration Database. *Sci. Data* **9**, 409 (2022).

58. Zhang, Y. et al. A global moderate resolution dataset of gross primary production of vegetation for 2000–2016. *Sci. Data* **4**, 170165 (2017).

59. Li, X. & Xiao, J. Mapping photosynthesis solely from solar-induced chlorophyll fluorescence: A global, fine-resolution dataset of gross primary production derived from OCO-2. *Remote Sens.* **11**, 2563 (2019).

60. Jung, M. et al. Compensatory water effects link yearly global land CO₂ sink changes to temperature. *Nature* **541**, 516–520 (2017).

61. Mu Q., Zhao M., Running S. W. MODIS Global Terrestrial Evapotranspiration (ET) Product (NASA MOD16A2/A3) Collection 5. NASA Headquarters. Numerical Terradynamic Simulation Group Publications. 268. https://scholarworks.umt.edu/ntsg_pubs/268. (2013).

62. Zhang, Y. et al. Coupled estimation of 500 m and 8-day resolution global evapotranspiration and gross primary production in 2002–2017. *Remote Sens. Environ.* **222**, 165–182 (2019).

63. Wang, X. et al. No trends in spring and autumn phenology during the global warming hiatus. *Nat. Commun.* **10**, 2389 (2019).

64. Dengel, S. & Grace, J. Carbon dioxide exchange and canopy conductance of two coniferous forests under various sky conditions. *Oecologia* **164**, 797–808 (2010).

65. Blanken, P. & Black, T. A. The canopy conductance of a boreal aspen forest, Prince Albert National Park, Canada. *Hydrolog. Process.* **18**, 1561–1578 (2004).

66. Liu, H. et al. Annual dynamics of global land cover and its long-term changes from 1982 to 2015. *Earth Syst. Sci. Data* **12**, 1217–1243 (2020).

Acknowledgements

The work was supported by the National Natural Science Foundation of China (Grant No. 42220104009 to C.S.; 42101109 to N.C.; 42271122 to L.S.), the Jilin Provincial Natural Science Foundation to N.C. (Grant No. YDZJ202201ZYTS477), and the China Postdoctoral Science Foundation-funded project to N.C. (Grant No. 2020M681058; 2022T150644). X.X. has been supported by the U.S. National Science Foundation (2145130).

Author contributions

N.C. and X.X. designed the study. N.C. performed the analysis. Y.Z., C.S. and X.W. contributed the field data. N.C. and X.X. wrote the paper with input from all coauthors. F.Y., M.X., Q.W., G.H., T.B., Y.Z., J.L., T.Z., Y.S., L.S., Y.G., H.Z., G.M., and Y.D. provided method suggestions and contributed to the interpretation of the results.

Competing interests

The authors declare no competing interests.

Additional information

Supplementary information The online version contains supplementary material available at <https://doi.org/10.1038/s41467-023-42932-w>.

Correspondence and requests for materials should be addressed to Changchun Song, Xiaofeng Xu or Xianwei Wang.

Peer review information *Nature Communications* thanks Meng Zhao, and the other, anonymous, reviewer(s) for their contribution to the peer review of this work. A peer review file is available.

Reprints and permissions information is available at <http://www.nature.com/reprints>

Publisher's note Springer Nature remains neutral with regard to jurisdictional claims in published maps and institutional affiliations.

Open Access This article is licensed under a Creative Commons Attribution 4.0 International License, which permits use, sharing, adaptation, distribution and reproduction in any medium or format, as long as you give appropriate credit to the original author(s) and the source, provide a link to the Creative Commons license, and indicate if changes were made. The images or other third party material in this article are included in the article's Creative Commons license, unless indicated otherwise in a credit line to the material. If material is not included in the article's Creative Commons license and your intended use is not permitted by statutory regulation or exceeds the permitted use, you will need to obtain permission directly from the copyright holder. To view a copy of this license, visit <http://creativecommons.org/licenses/by/4.0/>.

© The Author(s) 2023